Kobe University Repository : Kernel

PDF issue: 2025-12-05

Bistatic Ocean Wave Remote Sensing System by GPS

Cui, Jian
Kouguchi, Nobuyoshi

(Citation)
IEICE Transactions on Communications,96(6):1625-1632

(Issue Date)
2013-06-01

(Resource Type)
journal article

(Version)
Version of Record

(Rights)
copyright©2013 IEICE

(URL)
https://hdl.handle.net/20.500.14094/90002995

PAPER

Bistatic Ocean Wave Remote Sensing System by GPS

Jian CUI[†], *Nonmember and* Nobuyoshi KOUGUCHI[†a)], *Member*

SUMMARY This paper presents a bistatic remote sensing system to efficiently estimate the characteristics of sea swell near a harbor by receiving and processing global navigation satellite system signals transmitted in line-of-sight channels and fading multipath channels. The new system is designed to measure and monitor sea swell to improve the safety of mooring and navigation services in or around harbors, and long-term measurement also will provide valuable hydrologic data for harbor construction or reconstruction. The system uses two sets of antennas. One is a conventional antenna to receive line-of-sight signal and mitigate the disturbances from multiple propagation paths, and the other is a left hand circular polarization arrayed antenna to receive reflected signals from sea-surface. In particular, a wide bandwidth RF/IF front-end is designed to process reflected signals with high sampling frequency. A software receiver is developed to provide information from satellites and line-of-sight signals, and a wave characteristic estimator is also developed to process reflected signals. More specifically, correlators and Teager-Kaiser energy operator are combined to detect and depict reflected signals. Wave propagation of sea swell can be accurately mapped using intensity and relative time delays of reflected signals. The operational performance of the remote sensing system was also evaluated by numerical simulations. The results confirm that wavelength and wave period can be measured precisely by the proposed bistatic ocean wave remote sensing system.

key words: *GPS signal, arrayed antenna, ocean wavelength, wave period, wave direction*

1. Introduction

Harbors are places where vessels can moor securely. Unfortunately, most harbors are continually subjected to long period waves generated on the open sea and, that enter the harbor with great energy. Large vessels are more apt to be disturbed by long period waves that cause large motions [1], [2]. Long period waves also impose irregular course deviations on vessels navigating the harbor entrance channel. Moreover the effectiveness of breakwaters and jetties to long period waves is limited [3]. Long period waves have seriously hampered the secure and efficient use of harbors. Incident wave energy into a harbor is associated with wave characteristics such as wave height, wavelength and incidence direction. As a result, ocean wave measurements of long period waves are required to investigate wave characteristics for harbors in use or under construction.

In general, ocean wave measurements are made with different types of instruments such as high frequency (HF) radar, wave rider buoys and acoustic Doppler current profilers (ADCPs). Different ocean wave measurement instruments have their own advantages and disadvantages for different applications. Shore-based HF radar receives backscattered signals to retrieve sea-surface wave characteristics for coastal monitoring [4]–[6]. HF radar systems are usually built as large-scale systems operating on wide coastal areas over hundreds of square kilometers. Wave rider buoys have been extensively applied in ocean observation to collect wave characteristics. National Data Buoy Center (NDBC) of U.S.A. [7], [8] and Nationwide Ocean Wave Information Network for Ports and Harbors (NOWPHAS) of Japan [9] observe ocean waves with large networks of buoys. ADCPs are deployed beneath the sea-surface to measure wave and current [10], [11]. Buoy systems and ADCPs, however, suffer damage from floating debris and large waves, and maintenance is always troublesome. Recently developed Global Navigation Satellite Signals Reflectometry (GNSS-R) techniques provide an efficient method to retrieve sea-surface height [12] and characteristics of the surface wind [13] from reflected GPS signals. However, receivers usually are carried by airplane or satellite to collect signals from wide areas, and it is also not easy to measure detailed characteristics of ocean waves from such height, such as wave length, wave period and wave direction. Therefore, an easy and efficient ocean wave measurement system should be developed to estimate detailed wave characteristics of long period waves inside and outside harbors.

This paper presents an ocean wave remote sensing system that measures wave characteristics by GPS signals. Long period waves with periods ranging from 10 to several tens of seconds are targeted by this system. Called sea swell, they are frequently generated by a storm kilometers or even hundreds of kilometers away from a harbor; they retain a relatively uniform wave shape as they propagate. The remote sensing system is fixed near a harbor to receive GPS signals transmitting in a line-of-sight (LOS) channel and multipath (MP) channel from the sea-surface. Because the remote sensing measurement is based on wave shape and propagation, characteristics of sea swell can be extracted almost immediately even if the multipath channel is severely fading. Furthermore, the remote sensing system can provide a continuous long-term measurement for the sea area near harbors under bad weather conditions. The system construction and installation are also relatively easy to carry out.

The proposed remote sensing system uses two sets of antennas. A conventional antenna and a left hand circular

Manuscript received June 18, 2012.
Manuscript revised December 17, 2012.
[†]The authors are with the Graduate School of Maritime Sciences, Kobe University, Kobe-shi, 658-0022 Japan.
a) E-mail: kouguchi@maritime.kobe-u.ac.jp
DOI: 10.1587/transcom.E96.B.1625

Copyright © 2013 The Institute of Electronics, Information and Communication Engineers

polarization (LHCP) arrayed antenna receive GPS signals of LOS channel and multipath channel respectively. Two front-ends work with very high sampling frequency and the front-end, processing reflected signals, features relatively wide bandwidth (BW) to pass more reflected signal energy. The software receiver and wave characteristic estimator analyze two digitalized intermediate frequency (IF) signals respectively.

Wave height measurement has been successfully measured using variations of GPS antenna height [14], [15]. This paper concentrates on how to measure wavelength, wave period and direction. Section 2 introduces the outline of the whole system with emphasis on the design and operation of the arrayed antenna, the wide bandwidth front-end and the wave characteristic estimator along with the standard software receiver. A detailed processing method using correlators and Teager-Kaiser energy operator (TKEO) [16], [17] is presented in Sect. 3. Finally, Sect. 4 presents the results of numerical simulation to explain system validity and performance.

2. Remote Sensing System

2.1 Outline of System

The remote sensing system is sketched in Fig. 1. A GPS satellite flying over the sea-surface is transmitting GPS signals and the sea-surface reflects some signals forward. As a result, the GPS signals in the LOS channel and the multipath channel are received by an upward conventional antenna and an LHCP arrayed antenna facing the sea-surface respectively. Two sets of front-ends, labeled LOS and MP, convert received GPS signals from RF signals to IF digital signals. The software receiver tracks the motions of satellites and provides necessary information to the wave characteristic estimator. The wave characteristic estimator is therefore able to generate accurate results.

In practice, wavelength and wave direction need to be measured using at least two remote sensing systems configured as in Fig. 2, in which each arrayed antenna denotes one remote sensing system. Aiming at an identical sea-surface, two remote sensing systems generally tend to produce different results of wavelength |PA| and |PB| because the directions of these two systems don't necessarily measure true wave direction. Obviously, if a parallelogram PACB is established on the surface of the sea with two adjacent sides |PA| and |PB| determined by measuring their resultant wavelengths and the intersection point is P fixed by the directions of the two systems, and its diagonal |PC| pointing to seashore just points to the true wave direction and a half-length of this diagonal, |PO|, is considered as the true wavelength. These two systems are identical, so in the following sections, the remote sensing processing method will be elaborated using one of them.

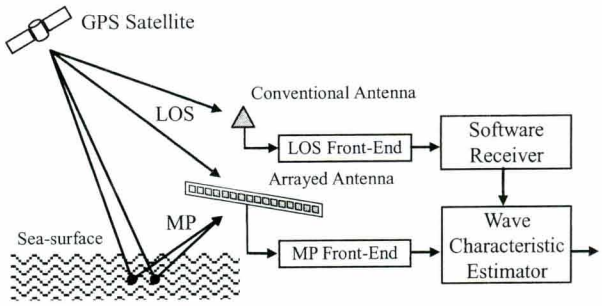

Fig. 1 Outline of proposed system.

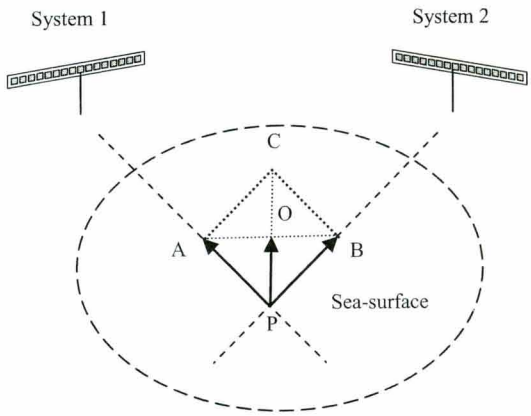

Fig. 2 Configuration of two systems.

2.2 Arrayed Antenna

The remote sensing system operates in a multipath environment in which reflected signals of the sea-surface are mixed with ones from the surroundings. Therefore a linear array of GPS antennas should be utilized, which can receive signals from the desired direction. Here, the arrayed antenna is designed with 16 elements of patch LHCP antennas in a horizontal array in series and the interval of each element is half the wavelength of the GPS signals. The electric field intensity is calculated with the following equation [18] where θ is angle of direction.

$$E = \frac{\cos\left[\frac{\pi}{2}\cos(\theta)\right]}{\sin(\theta)} \times \frac{\sin(\theta)[8\pi\cos(\theta)]}{\sin\left[\frac{\pi}{2}\cos(\theta)\right]} \tag{1}$$

The directional pattern of the arrayed antenna in Fig. 3 shows the relative intensity of GPS signals received from the front. A narrow fan beam perpendicular to the antenna surface is obtained, which provides the basis for receiving reflected signals from the sea-surface and suppressing signals from the side. Therefore, the arrayed antenna can only receive reflected signals of one visible satellite in main beam, and reflected signals of other satellites are largely attenuated. The directional pattern is utilized in the following numerical simulation and manifested in the reflected signal intensities. During measurement, the position of the visible satellite is provided by a software receiver as shown in Fig. 1

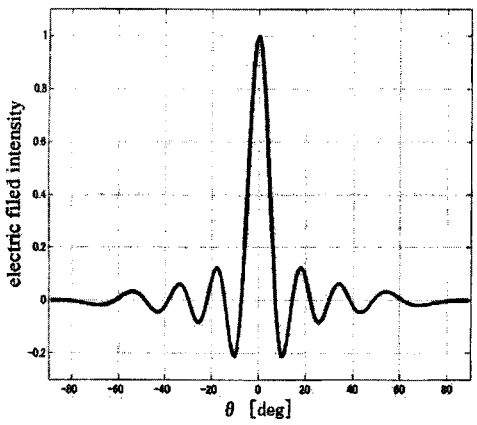

Fig. 3 Normalized directional pattern of arrayed antenna.

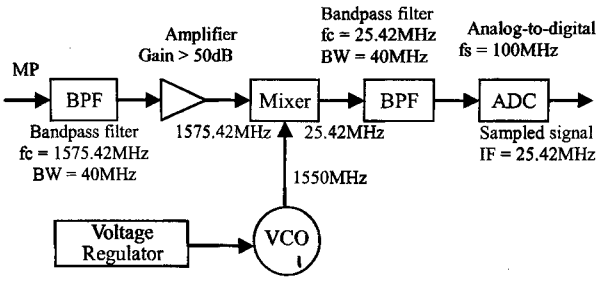

Fig. 4 Signal flow of front-end.

and the direction of the arrayed antenna is also manifested by an additional compass, with which the arrayed antenna is adjusted to keep the visible satellite in the main beam.

2.3 Front-End

In remote sensing system, the MP front-end is designed to process signals of wider bandwidth that permits more reflected signal energy to go through. A block diagram of the MP front-end is shown in Fig. 4.

The first component is a bandpass filter (BPF). The GPS signal format is a direct sequence spread spectrum and the GPS signal lies well below the noise floor [19], so the front-end has to attenuate out-of-band noise with a bandpass filter. Furthermore, a sharper correlation peak is achieved by broadening the receiver bandwidth [20]. As a result, a 40 MHz bandpass filter [21] is used to pass signal with a center frequency (f_c) of 1575.42 MHz. The GPS signal power after the first BPF filter is so weak that it is not enough to be processed by components following, unless an amplifier with over 50 dB gain is used to raise the weak signal to an appropriate magnitude. A voltage controlled oscillator (VCO) generates 1550 MHz oscillator signals for Mixer in which the GPS signal is down-converted to an intermediate frequency (f_{IF}) 25.42 MHz. The second BPF retains IF component and removes ultra-high frequency components from the output of the Mixer. An analog-to-digital converter (ADC) with 100 MHz sampling frequency (fs) is adopted to sample 40 MHz bandwidth signals.

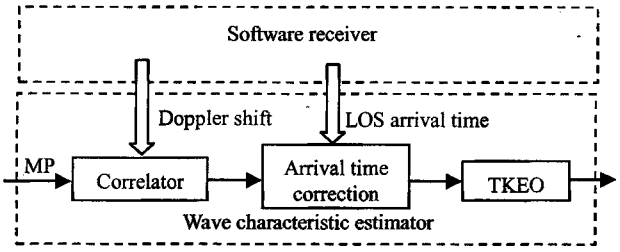

Fig. 5 Functional modules of wave characteristic.

2.4 Wave Characteristic Estimator

The software receiver in Fig. 1 processes LOS signals to provide real-time satellite information such as arrival time of LOS signal, azimuth, elevation and Doppler frequency shifts of visible satellites to the wave characteristic estimator.

Figure 5 shows the main functional modules of the wave characteristic estimator. The correlator resolves correlations for every received millisecond signal efficiently. Arrival times of the LOS signal are also estimated and transferred from the software receiver to the wave characteristic estimator as a time reference to align the arrival times of reflected signals.

Usually, a group of obvious peaks will appear in the correlator output, and a certain of them denotes arrival times of the reflected signals and naturally the others are noise. Generally the multipath arrival time cannot be identified from a single correlator result because of the low level of carrier-to-noise-density ratio (C/N_0). After the arrival time correction, averaging of correlator results can be used to reduce the noise.

3. Wave Characteristic Estimator

3.1 Received Signal

Multipath arrival time is delayed due to its longer propagation path than the LOS signal. Therefore, relative time delay is available to identify multiple propagation paths. In order to explain the measurement method briefly, the case of a single frequency ocean wave will be discussed in this section. A wave surface containing many frequency components will be generated and used for sea swell measurement in a numerical simulation. The following Fig. 6 shows an arrayed antenna receiving three relatively strong signals reflected from P1, P2 and P3 on the crest of ocean waves, labeled MP1, MP2 and MP3.

In general, the composite signal received by the antenna array is expressed by the simplified expression as follows,

$$x^k(t) = \sum_{i=1}^{3} A_i(t)C^k(t-\tau_i(t))D^k(t-\tau_i(t)) \cos(2\pi(f_0 + v_i(t))t + \varphi_i(t)) + e(t) \quad (2)$$

where,

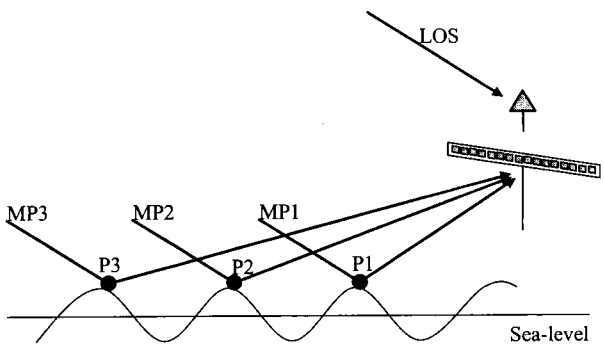

Fig. 6 Receiving aspect near sea-surface.

x: Composite received signal;
k: Satellite number;
A_i: Amplitude of the ith component;
D: Navigation data;
C: C/A code;
f_0: L1 carrier frequency;
τ_i: Relative time delay of the ith component to LOS;
v_i: Frequency change of the ith component;
ϕ_i: Carrier phase offset of the ith component;
e: Noise.

The received signal $x(t)$ is then filtered, amplified and down converted in the wide bandwidth front-end. Let $y(t)$ denote the output of the Mixer, let B_i denote resultant amplitude of each multipath component, then $y(t)$ is expressed as

$$y^k(t) = \sum_{i=1}^{3} B_i(t)C^k(t-\tau_i(t))D^k(t-\tau_i(t)) \cos(2\pi(f_{IF}+v_i(t))t+\varphi_i(t))+e(t) \quad (3)$$

This signal is then sampled by ADC, described as

$$y^k(n) = \sum_{i=1}^{3} B_i(n)C^k(n-m_i(n))D^k(n-m_i(n)) \cos(2\pi(f_{IF}+v_i(n))n+\varphi_i(n))+e(n) \quad (4)$$

with n in units of $1/fs$ seconds; n indicates the signal is discrete in time. m_i is the number of samples for relative time delay to LOS signal, $m_i = \tau_i/fs$.

3.2 Correlator and Teager-Kaiser Energy Operator

Here, suppose C/A code components have been demodulated from Eq. (4) for satellites k. Let $C^k(0)$, $C^k(m_i)$ denote a C/A code of LOS signal without time delay and a C/A code of ith multipath component with relative time delay m_i respectively, and let $C^k(m)$ denote a locally generated C/A code with time delay m. According to the autocorrelation property of C/A code, the autocorrelation between $C^k(0)$ and $C^k(m)$ is formulated as

$$r_0^{kk}(m) = \sum C^k(0)C^k(m), \quad and \begin{cases} r_{LOS}^{kk}(m) \approx 0 & m \neq 0 \\ r_{LOS}^{kk}(m) = \frac{fs}{1000} & m = 0 \end{cases} \quad (5)$$

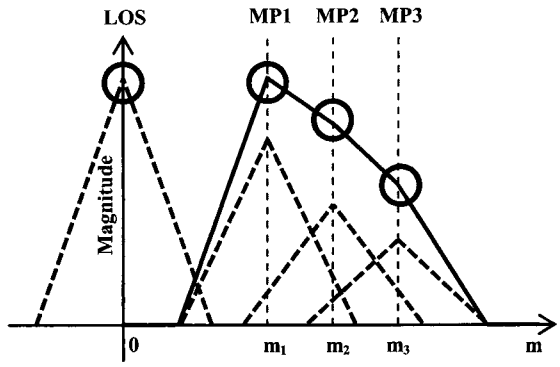

Fig. 7 Correlator output for reflected signals.

and the autocorrelations between $C^k(m_i)$ and $C^k(m)$ are

$$r_i^{kk}(m) = \sum C^k(m_i)C^k(m), \quad and \begin{cases} r_i^{kk}(m) \approx 0 & m \neq m_i \\ r_i^{kk}(m) = \frac{fs}{1000} & m = m_i \end{cases} \quad (6)$$

where r denotes correlation of C/A code.

Usually f_s is so much greater than 1000 that high correlation values can be obtained for satellite k when locally generated C/A code is aligned perfectly with incoming C/A codes. In Fig. 6, the different signal intensities of the LOS signal and the three reflected signals result in peaks of different magnitude. Therefore, four equilateral triangle peaks with different magnitudes are illustrated with broken lines in Fig. 7. Here, let a_0, a_1, a_2, a_3 denote coefficients to adjust the correlation values of LOS signal and the three reflected signals and $a_0 > a_1 > a_2 > a_3$. Consequently the correlation between C/A codes of LOS signal and locally generated C/A code is

$$r_{LOS}^{kk} = a_0 r_0^{kk}(m) \quad (7)$$

and the correlation between C/A codes of composite reflected signal and locally generated C/A code is

$$r_{MP}^{kk}(m) = a_1 r_1^{kk}(m) + a_2 r_2^{kk}(m) + a_3 r_3^{kk}(m) \quad (8)$$

Because the time length of one correlation peak is about double the time length of one chip of C/A code, three correlation peaks are usually superimposed to be a polyline for a composite received signal, shown as solid lines in Fig. 7. Three peak points are circled and m_1, m_2 and m_3 are considered as relative time delays of MP1, MP2 and MP3 to LOS.

In practice, too much noise is included in the received signal so the peaks are hard to pick out from correlator output. Therefore the discrete time Teager-Kaiser energy operator is used as an effective tool to highlight correlation peaks. Teager-Kaiser energy operator can be a high-pass filter [22]. The TKEO for the above-mentioned correlator output is calculated by

$$TKEO(m) = r^{kk}(m)^2 - r^{kk}(m-1)r^{kk}(m+1) \quad (9)$$

The TKEO for the LOS correlator output in Fig. 7 is

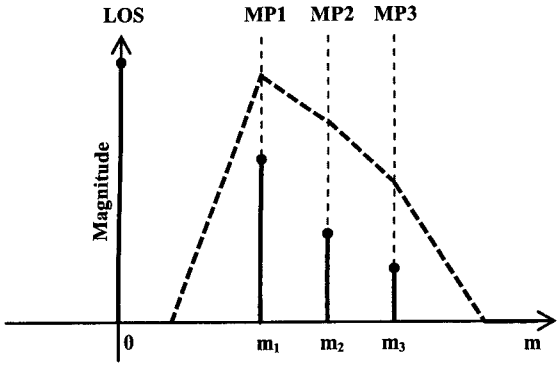

Fig. 8 TKEO output for reflected signals.

$$TKEO(m) = \begin{cases} 2r^{kk}_{LOS}(0)\delta - \delta^2 & m = 0 \\ \delta^2 & m \text{ at peak side} \\ 0 & m \text{ out of peak} \end{cases} \quad (10)$$

where δ is the magnitude of difference between two consecutive sampling instants on the LOS correlation peak side, i.e. taken anywhere below the magnitude of the peak point. To compare TKEO values between peak point and peak side with

$$\frac{TKEO(0)}{\delta^2} = \frac{2r^{kk}_{LOS}(0)}{\delta} - 1 \quad (11)$$

a large value is usually yielded so that an obvious impulse appears at zero. Similarly, TKEO for reflected signal correlation can be resolved and then the results are shown in Fig. 8.

In comparison between Fig. 7 and Fig. 8, three outstanding peaks of the TKEO output are obtained and then each number of samples for relative time delay to LOS signal m_1, m_2 and m_3 can be estimated clearly.

3.3 Estimation of Wavelength and Wave Period

For an estimation of the wavelength and wave period, each number of samples m_1, m_2 and m_3 are transferred to the distance from the arrayed antenna to the reflection point. The horizontal distances from the arrayed antenna to the reflection points are calculated using the geometrical relationship of the receiving condition near sea-surface in Fig. 6. Let $\angle$E be the satellite elevation angle, h be the antenna height and c be light speed, and the horizontal distance d from the position of the arrayed antenna to the reflection point is calculated as follows,

$$d_i = h\tan\left(2\arctan\left(\frac{\frac{m_i c}{f_s h} - \sin\angle E - \sqrt{\rho}}{1 + \cos\angle E}\right)\right)^{-1} \quad (12)$$

where, $\rho = (\frac{m_i c}{f_s h})^2 - \frac{2m_i c}{f_s h}\sin\angle E$.

In Eq. (12), let the wavelength be 200 meters and the wave period be 20 seconds, and let the elevation angle of the satellite be 25 degrees and the antenna height be 50 meters, the horizontal distance d from the arrayed antenna to the reflection point is indicated as the vertical axis in Fig. 9.

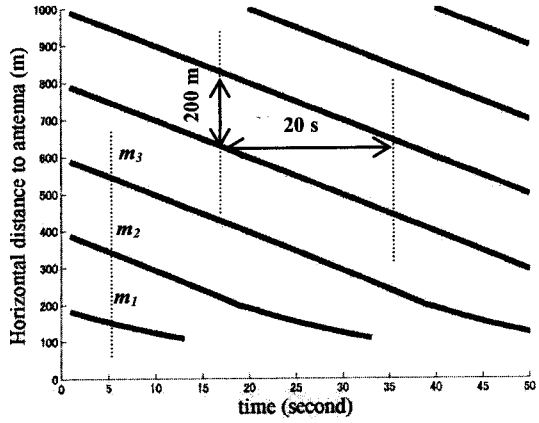

Fig. 9 Time series alignment of TKEO output.

In this figure, the horizontal axis is the measurement time, and seven lines show the seven peaks of the TKEO outputs. Consequently, the horizontal span between the two lines shows the wave period, and the vertical span between two lines indicates the wavelength in the direction of the arrayed antenna.

4. Numerical Simulations

4.1 Simulation Conditions

Table 1 shows the conditions of our numerical simulation, such as the status of satellites, the characteristics of ocean wave and the installation of antenna. The ocean wave characteristics are selected from a relatively long period sea swell [23].

Considering noise environment, the carrier to noise ratio, C/N_0, should be determined, since it varies due to channel conditions. Here, the C/N_0 is calculated as follows,

$$C/N_0 = 10\log_{10}\left(\frac{P_s}{P_n}\right). \quad (13)$$

where Ps and P_n are signal power received by the arrayed antenna and noise power. Usually −160 dBW carrier power at the Earth's surface [24] and −204 dBW noise power are used to generate GPS signals and white Gaussian noise [25].

4.2 Reflected Signals from Sea-Surface

4.2.1 Wave Model

A wave spectrum model of approximately natural sea swell is calculated from sea-surface near the reflection point suitable for microwave propagation and an equation of swell spectrum is calculated as follows [26], [27],

$$F(k) = \frac{H_s^2}{16\sqrt{2\pi}\sigma_l}\exp\left[-\frac{1}{2}\left(\frac{k - k_{peak}}{\sigma_l}\right)^2\right] \quad (14)$$

where H_s is a significant wave height, k_{peak} is the wave number of the spectral peak and σ_l is the spectrum width.

Table 1 Simulation conditions.

	Characteristic	Value
Simulation time	resolution	0.25 ns
Sea-surface	facet	1 m^2
GPS Satellite	elevation	25 deg.
	azimuth	180 deg.
Ocean Wave (Sea swell)	water depth	10 m
	period	20 s
	length	200 m
	significant height	2 m
	direction	0 deg.
Arrayed Antenna	antenna height	50 m
	direction	face to satellite

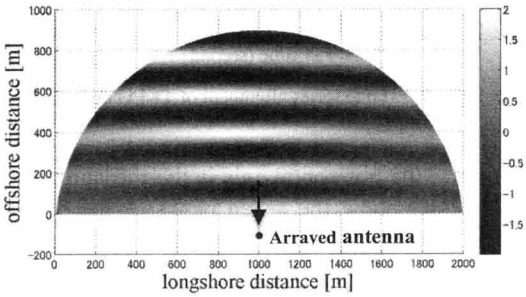

Fig. 10 One example of calculated sea-surface.

Figure 10 shows one example of the calculated sea-surface. This sea-surface model is defined by an arc from a 1,000 meters radius circle centered at the position of the arrayed antenna, with the area below straight line (parallel to the arrayed antenna) passing through the specular reflection area, removed. In this sea-surface area, some swells exist. The bright areas are the crests of the sea swells and the dark areas are the troughs of the sea swells. The arrow indicates the wave direction and the black point mark is the position of the arrayed antenna. It is necessary to mask the signals from the specular reflection point to the arrayed antenna, because the signals have the same relative time delays as the signals reflected from the modeled sea-surface.

4.2.2 Scattering Pattern

The incoming signals to the modeled sea-surface are reflected as a scattering pattern of the wave surface. According to the practical remote sensing environment on rough sea-surface, a scattering pattern model of the bi-directional reflectance distribution function is defined by the following equation [28].

$$R \propto (\cos\theta_0 \cos\theta_1)^{k-1} \frac{1-g^2}{(1+2g\cos\Theta+g^2)^{3/2}} \tag{15}$$

where, $\cos\Theta = \cos\theta_0 \cos\theta_1 + \sin\theta_0 \sin\theta_1 \cos(\phi_1 - \phi_0)$, and
θ_0: incidence angle, $[0, \pi/2]$;
θ_1: scattering angle, $[0, \pi/2]$;
k: factor of intensity along normal direction, $[1, \infty]$;
g: anisotropy factor, $(-1, 1)$;
Θ: scattering phase angle;
ϕ_0: azimuth angle of satellite, $[0, \pi]$;
ϕ_1: azimuth angle of reflection, $[0, \pi]$.

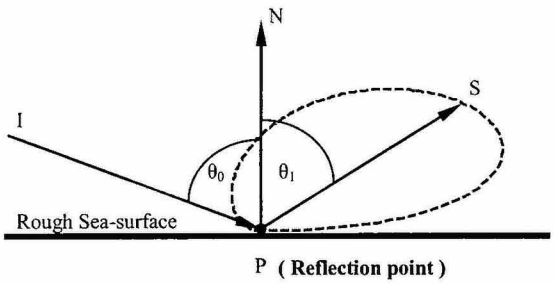

Fig. 11 Scattering pattern from point P.

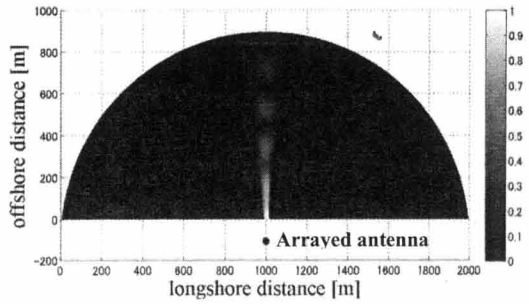

Fig. 12 Normalized reflected signal intensities.

Figure 11 shows a scattering pattern from the reflected point P. In this figure, the incidence signal is "I", the normal direction of the scattering surface is "N", the direction to the antenna point is "S" and the scattering pattern from Eq. (15) is shown by dashed lines. In Eq. (15), the coefficients "k" and "g" are respectively equal to 2 and 0.7, and $\varphi_1 - \varphi_0$ and θ_0 become π and $7\pi/18$. The scattering coefficient "R" is decided by the magnitude of the scattering pattern from point "P" on the sea-surface.

4.2.3 Normalized Reflected Signal Intensities

After each antenna input signal with a relative time delay and scattering coefficient has been combined along with the directional pattern of the arrayed antenna, the received signal at the arrayed antenna is calculated in next equation [29]. Let (i, j) be the coordinates of the reflected point on the sea-surface.

$$x_{i,j}(t) = \frac{1}{\sqrt{2\pi} d_{i,j}(t)} R_{i,j}(t) E_{i,j}(t) MP(t - \tau_{i,j}) \tag{16}$$

where attenuation factors $d_{i,j}(t)$ is the distance from the reflection point coordinate (i, j) to the antenna, $R_{i,j}(t)$ is the scattering coefficient at the reflection point, and $E_{i,j}(t)$ is the electric field intensity of the incident wave at coordinate (i, j). $\tau_{i,j}$ is a time delay, and $MP(t - \tau_{i,j})$ is the reflected signal from the sea surface with time delay $\tau_{i,j}$. Equation (16) without time delay $\tau_{i,j}$ can be seen with the normalized received signal intensities on the modeled sea-surface illustrated in Fig. 12.

From Fig. 12, there are many reflected signals of strong intensities in the white area, and there are many reflected signals of weak intensities in the black area. The received

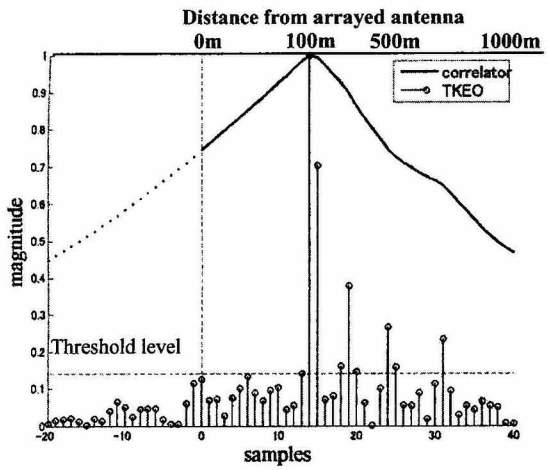

Fig. 13 Normalized correlator and TKEO output.

signal at the arrayed antenna is calculated by considering the time delay of the reflected signal, $\tau_{i,j}$. As the variations of the strong and weak signals are consistent with the significant wavelengths of the simulated sea swell and the strong and weak signals have different time delays, the wavelengths of the modeled sea swell in the direction of the received antenna can be measured.

4.3 Estimation for Wave Characteristics

4.3.1 Correlator and Teager-Kaiser Energy Operator

Figure 13 shows one example of the correlator and TKEO output signals. In this figure, the solid line shows the correlator output and a series of bars show the TKEO outputs. The highest bar of the TKEO output is the most significant reflected signal from the near specular reflection area, which indicates 107 meters on the horizontal axis and shows the relative time delay from the LOS signal. The higher TKEO output peaks located on the right side of the highest bar are reflected signals from the measurable sea-surface.

4.3.2 Estimation of Wave Length and Period

The TKEO output signals are arranged in a measurement time series in reference to Fig. 9. In Fig. 14, TKEO output signals are lined up, and the magnitude of TKEO outputs are shown by the gray scale, and the white area shows the strong reflected signals from the measureable sea-surface. In Fig. 14, we found several white areas that show a tendency of downward-sloping above the specular reflection area that is above 100 meters on the vertical axis.

From the viewpoint of estimation for wave characteristics, the TKEO outputs are binarized. In Fig. 13, there are no reflected signals before the highest bar of the TKEO output, and the triple standard deviation value of the TKEO output in the noise area is selected as a threshold level for a binarization. Figure 15 shows the binarized results of the TKEO outputs in Fig. 14. From the binarization results in

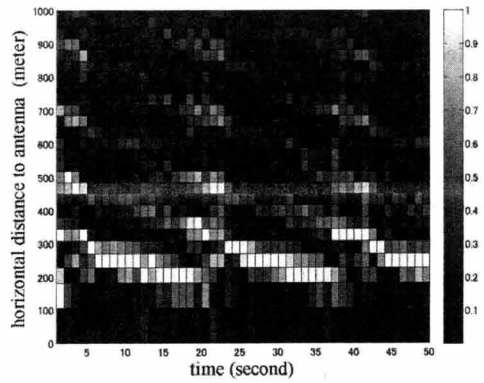

Fig. 14 Time series alignment of TKEO output.

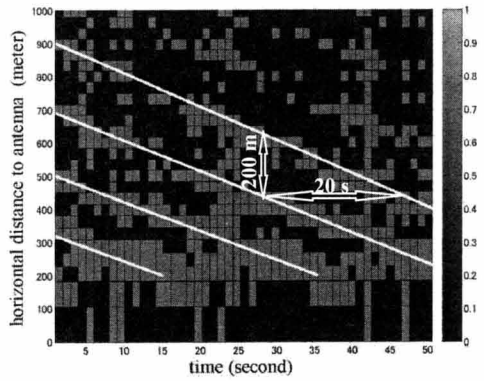

Fig. 15 Binalized time series alignment of TKEO output.

Fig. 15, the wavelength and wave period can be estimated to be about 200 meters and 20 seconds respectively.

5. Conclusion

A bistatic ocean wave remote sensing system consisting of an arrayed antenna, front-ends and wave characteristic estimator was proposed. The arrayed antenna received the signals from its facing direction, and was configured to form a very narrow fan beam directional pattern. The front-end with wider bandwidth was designed to identify sequentially reflected signals from the measurable sea-surface. The correlator and TKEO outputs, which were obtained by the wave characteristic estimator to identify relative time delays of reflected signals, estimate the wavelength and wave period in the direction of the arrayed antenna. Additionally two remote sensing systems can estimate the true wave direction and wavelength by means of the composition of each vector component.

A numerical simulation was executed to evaluate the capability of the proposed remote sensing system. According to simulation results, the wavelength and the wave period of the specified sea swell can be estimated. Consequently, the proposed system is available and efficient to estimate wavelength, wave period and wave direction of the sea swell of long periods.

Acknowledgments

We would like to acknowledge the help of Professors Yasuo Arai and Shigeyuki Okuda of Marine Technical College for providing with valuable guidance and effective advices in this research, and great thanks to Mr. Akihiro Ikawa for his direction and assistance in every experiment and heartfelt thanks to all schoolmates for their support and encouragement.

References

[1] S. Kery, "The development of ocean surface wave climatology in support of ship to ship connected transfer of cargo and personnel," OCEANS, Proc. MTS/IEEE, pp.251–256, Bei Jing, 2005.

[2] H. Kashima, K. Hirayama, K. Haruo, T. Hiraishi, and K. Nakai, "Consideration of design wave for port construction according recent observation," OCEANS 2008 — MTS/IEEE Kobe Techno-Ocean, pp.1–6, 2008.

[3] C.K. Young, Handbook of Coastal and Ocean Engineering, World Scientific Publishing, 2009.

[4] L.R. Wyatt, S.P. Thompson, and R.R. Burton, "Evaluation of high frequency radar wave measurement," Coastal Engineering, vol.37, no.3-4, pp.259–282,1999.

[5] V. Cees, A. Reniers, J. Atanga, A. Vizinho, and J. Vogelzang, "Monitoring surface waves in coastal waters by integrating HF radar measurement and modeling," Coastal Engineering, vol.37, no.3-4, pp.431–453, 1999.

[6] S.B. Jonathan, L.H. Malcolm, and P. Arnstein, "A method of swell-wave parameter extraction from HF ocean surface radar spectra," IEEE J. Ocean. Eng., vol.31, no.4, pp.812–818, 2006.

[7] P.A. Work, "Near shore directional wave measurements by surface-following buoy and acoustic doppler current profiler," Ocean Engineering, vol.35, pp.727–737, 2008.

[8] J.C. McCall, "Advances in National Data Buoy Center technology," Proc. OCEANS'98 Conference, pp.544–548, 1998.

[9] K. Kawaguchi, M. Satoh, K. Seki, and H. Kawai, "Annual report on Nationwide Ocean Wave Information Network for Ports and Harbors (NOWPHAS 2010)," PARI Technical Note, 2012.

[10] E.A. Terray, B.H. Brumley, and B. Strong, "Measuring waves and currents with an upward-looking ADCP," Current Measurement, Proc. IEEE Sixth Working Conference, pp.66–71, 1999.

[11] R. Pinkel and J.A. Smith, "Open ocean surface wave measurement using Doppler sonar," J. Geophysical Research, vol.92, pp.12967–12973, 1987.

[12] Y. Kegen, R. Chris, and D. Andrew, "Sea surface altimetry based on airborne GNSS signal measurements," ISPRS Ann. Photogram. Remote Sens. Spatial Inf. Sci., I-7, pp.347–352, 2012.

[13] A. Komjathy, M. Armatys, D. Masters, and P. Axelrad, "Retrieval of ocean surface wind speed and wind direction using reflected GPS signals," J. Atmospheric and Oceanic Technology, vol.21, pp.515–526, March 2004.

[14] H.M. Bruce, "Modeling and simulation of GPS multipath propagation," the cooperative research center for satellites system Queensland University of Technology, pp.223–237, 2001.

[15] S. Okuda, Y. Arai, and N. Kouguchi, "Sea surface wave information using GPS sea reflected signal — Wave height," Institute of Navigation GNSS 18th International Technical Meeting of the Satellite Division, pp.810–815, Long Beach, CA, 2005.

[16] K. Eivind, "Signal processing using the Teager energy operator and other nonlinear operators," Candidatus Scient thesis, University of Oslo Department of Informatics, 2003.

[17] H. Ridha, R. Markku, and H. Taneli, "Teager-kaizer operator based filtering," Tenth European Signal Processing Conference, EUSIPCO'-2000, pp.545–1548, Tampere, Finland, 2000.

[18] J. Cui, N. Kouguchi, A. Ikawa, S. Okuda, and Y. Arai, "Wave remote sensing system by GPS," Proc. OCEANS 2010 IEEE, pp.1–7, Sydney, 2010.

[19] M.S. Braasch and A.J. Van Dierendonck, "GPS receiver architectures and measurements," Proc. Institute of Navigation GPS Meeting, vol.87, no.1, pp.48–64, 1999.

[20] NovAtel, "Discussions on RF signal propagation and multipath," Calgary, Alberta, Canada, T2E 8S5.

[21] J. Cui and N. Kouguchi, "Ocean wave observation by GPS signal," Proc. OCEANS 2011 IEEE, pp.1–7, Spain, 2011.

[22] V. Kandia and Y. Stylianou, "Detection of sperm whale clicks based on the Teager-Kaiser energy operator," Applied Acoustics, vol.67, pp.1144–1163, 2006.

[23] H. Mitsuyasu, Physics of Ocean Waves, Iwanami-Shoten, 1995.

[24] U.S. Government Department of Defense, Global Positioning System Standard Positioning Service Signal Specification, Second ed., p.9, June 1995.

[25] R.B. Langley, "GPS receiver system noise," GPS World, vol.8, no.6, pp.40–45, April 1997.

[26] S.L. Durden and J.F. Vesecky, "A physical radar cross-section model for a wind-driven sea with swell," IEEE J. Ocean. Eng., vol.10, pp.445–451, 1985.

[27] D. Hauser, E. Soussi, E. Thouvenot, and L. Rey, "SWIMSAT: A real-aperture radar to measure directional spectra of ocean waves from space — Main characteristics and performance simulation," Atmospheric and Oceanic Technology, vol.18, pp.421–437, 2001.

[28] H. Kuze, Y. Likuza, S.T. Akeuchi, and H. Yoshimori, Physical Principles of Remote Sensing, Second ed., pp.46–48, Cambridge University Press, 2005.

[29] J.G. Proakis, Digital Communications, Third ed., McGraw-Hill, 1995.

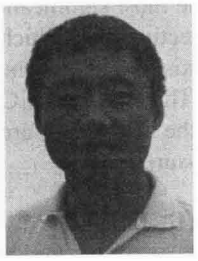

Jian Cui received the first Master's degree of Control Theory and Control Engineering in 2007 from Dalian Maritime University of China and the second Master's degree of Maritime Management Sciences in 2009 from Kobe University of Japan. Now, he is in pursuit of doctor's degree and his research field focuses on ocean wave observation by GPS signal.

Nobuyoshi Kouguchi received B.Sc. Degree of Maritime Science in 1978 from Kobe University of Mercantile Marine, and Ph.D. degree of Communication engineering in 1998 from Osaka University, From 1979 to 1991, he worked as an assistant and associate professor at Maritime Technical College. From 1992 to 2000, he was an associate professor at Kobe University of Mercantile Marine. He is currently a professor of Graduate school of Maritime Sciences, Kobe University. His interesting researches are ocean measurement science and technology, global navigation satellite system, and decision-making process of mariner.